NASA Technical Memorandum 2016-219219

March 2016

Passive Rocket Diffuser Theory:

A Re-Examination of Minimum Second Throat Size

Daniel R. Jones
Stennis Space Center, Mississippi

National Aeronautics
and Space Administration

NASA STI Program in Profile

Since its founding, NASA has been dedicated to the advancement of aeronautics and space science. The NASA scientific and technical information (STI) program plays a key part in helping NASA maintain this important role.

The NASA STI program operates under the auspices of the Agency Chief Information Officer. It collects, organizes, provides for archiving, and disseminates NASA's STI. The NASA STI program provides access to the NTRS Registered and its public interface, the NASA Technical Reports Server, thus providing one of the largest collections of aeronautical and space science STI in the world. Results are published in both non-NASA channels and by NASA in the NASA STI Report Series, which includes the following report types:

- TECHNICAL PUBLICATION. Reports of completed research or a major significant phase of research that present the results of NASA Programs and include extensive data or theoretical analysis. Includes compilations of significant scientific and technical data and information deemed to be of continuing reference value. NASA counter-part of peer-reviewed formal professional papers but has less stringent limitations on manuscript length and extent of graphic presentations.

- TECHNICAL MEMORANDUM. Scientific and technical findings that are preliminary or of specialized interest, e.g., quick release reports, working papers, and bibliographies that contain minimal annotation. Does not contain extensive analysis.

- CONTRACTOR REPORT. Scientific and technical findings by NASA-sponsored contractors and grantees.

- CONFERENCE PUBLICATION. Collected papers from scientific and technical conferences, symposia, seminars, or other meetings sponsored or co-sponsored by NASA.

- SPECIAL PUBLICATION. Scientific, technical, or historical information from NASA programs, projects, and missions, often concerned with subjects having substantial public interest.

- TECHNICAL TRANSLATION. English-language translations of foreign scientific and technical material pertinent to NASA's mission.

Specialized services also include organizing and publishing research results, distributing specialized research announcements and feeds, providing information desk and personal search support, and enabling data exchange services.

For more information about the NASA STI program, see the following:

- Access the NASA STI program home page at http://www.sti.nasa.gov

- E-mail your question to help@sti.nasa.gov

- Phone the NASA STI Information Desk at 757-864-9658

- Write to:
  NASA STI Information Desk
  Mail Stop 148
  NASA Langley Research Center
  Hampton, VA 23681-2199

NASA Technical Memorandum 2016-219219

March 2016

Passive Rocket Diffuser Theory:

A Re-Examination of Minimum Second Throat Size

Daniel R. Jones
Stennis Space Center, Mississippi

National Aeronautics
and Space Administration

ACKNOWLEDGEMENTS

The author would like to acknowledge NASA's RS-25 project for funding all work contained within this report. Further gratitude is extended to Dr. Daniel Allgood in recognition of his continued technical guidance and to Dr. Harry Ryan for his review of this paper.

ABSTRACT

Second-throat diffusers serve to isolate rocket engines from the effects of ambient back pressure during testing without using active control systems. Among the most critical design parameters is the relative area of the diffuser throat to that of the nozzle throat. A smaller second throat is generally desirable because it decreases the stagnation-to-ambient pressure ratio the diffuser requires for nominal operation. There is a limit, however. Below a certain size, the second throat can cause pressure buildup within the diffuser and prevent it from reaching the start condition that protects the nozzle from side-load damage. This paper presents a method for improved estimation of the minimum second throat area which enables diffuser start. The new 3-zone model uses traditional quasi-one-dimensional compressible flow theory to approximate the structure of two distinct diffuser flow fields observed in Computational Fluid Dynamics (CFD) simulations and combines them to provide a less-conservative estimate of the second throat size limit. It is unique among second throat sizing methods in that it accounts for all major conical nozzle and second throat diffuser design parameters within its limits of application. The performance of the 3-zone method is compared to the historical normal shock and force balance methods, and verified against a large number of CFD simulations at specific heat ratios of 1.4 and 1.25. Validation is left as future work, and the model is currently intended to function only as a first-order design tool.

NOMENCLATURE

A	Area
CFD	Computational Fluid Dynamics
D	Diameter
dr	Incremental Change in Radius
L	Length
$\dot{m}$	Mass Flow Rate
M	Mach Number
MW	Molecular Weight
NS	Normal Shock
OS	Oblique Shock
P	Pressure
R	Specific Gas Constant
r	Radius
T	Temperature
x	Axial Location
y+	Non-Dimensional Wall Spacing
α	Plume Expansion Angle
β	Oblique Shock Angle
γ	Ratio of Specific Heats
η	Nozzle Thrust Efficiency
θ	Angle
ν	Prandtl-Meyer Angle

SUBSCRIPTS

a	Ambient Condition
avg	Average
cell	Test Cell
DC	Diffuser Contraction
DI	Diffuser Inlet
i	Iteration Number
IMP	Impingement
INT	Intersection
min	Minimum
NE	Nozzle Exit
NS	Normal Shock
NT	Nozzle Throat
n	Component Normal to Oblique Shock
ST	Second Throat
Start	Start Condition
weighted	Weighted Average
0	Stagnation Condition
1,2,…	Station Number

BACKGROUND

The purpose of passive rocket diffusers is to enable testing of low P_{NE} engines at simulated altitude conditions without the additional cost and complexity of an ejector system. To accomplish this, they rely upon the inability of supersonic flow to relay pressure waves upstream. The rocket plume exits the nozzle and expands to the diffuser wall, thus isolating the engine from downstream pressure effects and providing a favorable pressure gradient at the nozzle lip. Boundary layer separation in the nozzle is avoided during steady-state operation, and the risk of

damage from unsteady pressure imbalances is substantially reduced. Passive diffusers can take several forms, each with their own advantages and disadvantages. Fig. 1 shows a selection of common varieties.

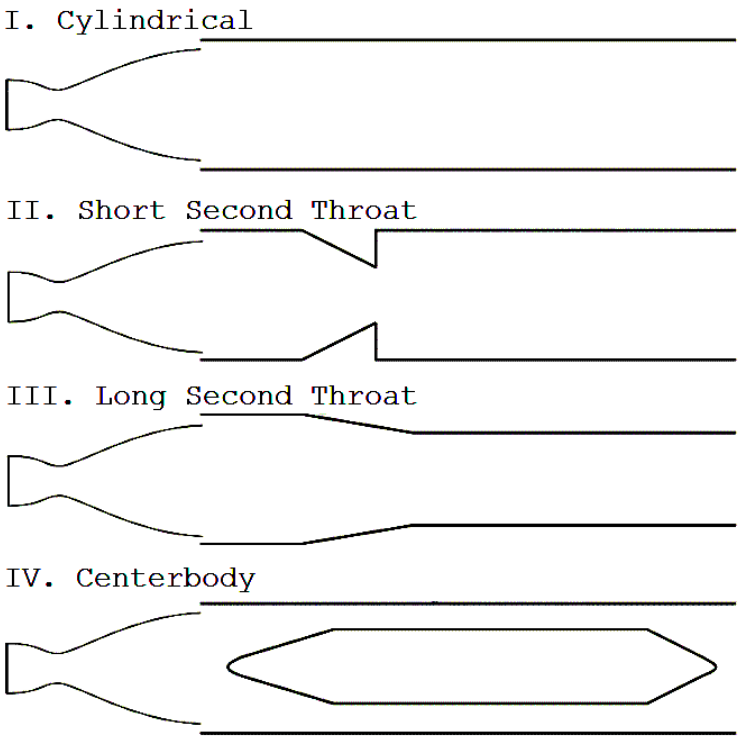

Fig. 1 – Passive Diffuser Geometries

Cylindrical diffusers are simple to design, construct, and keep cool, but their pumping performance is relatively poor. The addition of a contraction effectively decreases the P_0 required for a diffuser to operate against atmospheric back pressure. Short second throat diffusers (throat length-to-diameter ratio $[L/D]_{ST} < 1$) provide an improvement over cylindrical diffusers, and fix the separation point at the throat. However, their pumping performance is exceeded by long second throats ($[L/D]_{ST} > 5$), which provide something of a middle ground in the trade-off between performance and ease of design and construction. The main disadvantages of long second throat diffusers are their size and the possible introduction of strong oscillatory modes due to boundary layer separation becoming unstable when operating at sub-nominal pressure ratios. Centerbody diffusers are also able to provide relatively high pumping performance and can be comparatively compact. However, they can be difficult to design and keep cool as a result of the additional structure and stagnation points within the flow. This paper solely

focuses on second throat diffusers of $2.75 < [L/D]_{ST} < 8$ coupled with conical nozzles of $15^\circ \leq \theta_{NE} \leq 18^\circ$. Fig. 2 shows a typical geometry and the labels associated with each portion.

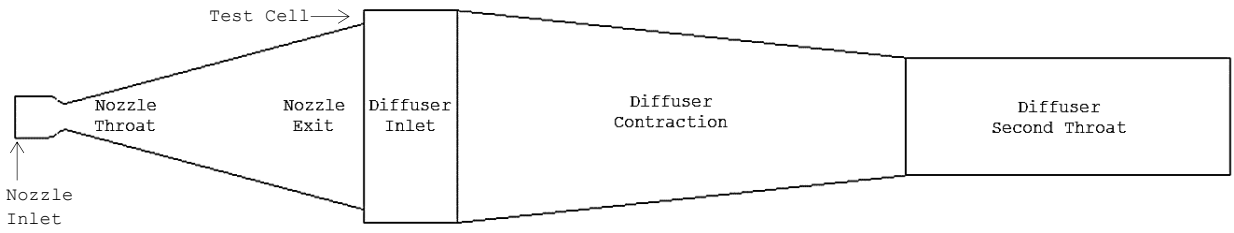

Fig. 2 – Second Throat Diffuser Terminology

Modes of Diffuser Operation

The following list establishes the terminology describing diffuser flow phenomena, broken into three categories based on the physical effects used to distinguish them. Not all are relevant to this report, but are included as an overview of diffuser operation. Fig. 3 displays the relationship between operating regimes, test cell pressure, flow structure, and second throat size for a typical diffuser geometry.

Flow Regimes Differentiated by Second Throat Effects

Choke: Flow within the diffuser throat is forced to sonic conditions. This is caused by very tight second throats and creates significant pressurization within the diffuser. The rocket nozzle is nearly guaranteed to incur boundary layer separation.

Non-Start: The plume exits the nozzle without attaching to the diffuser inlet, and supersonic flow exists in the diffuser throat. This is caused by a tight second throat or insufficient P_0/P_a. The nozzle may or may not experience boundary layer separation.

Marginal Start: The plume expands to and impinges upon the diffuser wall, but P_0/P_{cell} has not reached a constant value. This can be caused by the plume's impingement on the diffuser contraction.

Start: The plume expands from the nozzle and attaches to the diffuser wall. P_{cell} becomes directly proportional to P_0 (P_{cell}/P_0 = constant). This occurs only with sufficient minimum area and P_0/P_a.

Flow Regimes Differentiated by Back Pressure Effects

Separated: The diffuser is started, but the boundary layer separates at some point downstream of impingement. This mode of operation carries a high potential for unsteady flow and high local heat flux.

Full Flow: The diffuser is started and the boundary layer remains attached throughout its length. This regime provides steady-state operation and decreased heat flux compared to the separated condition.

Flow Regimes Differentiated by Transient Effects

Unstart: The temporary state of a start-capable-diffuser either before it achieves or after it loses its start condition. This is caused by low P_0 during system start and shut-down.

Hysteresis: The range of P_0/P_a that is unable to produce a start condition from quiescent initial conditions, but is able maintain start given an initial state in which the diffuser is already started. Shown in Fig. 4 as the difference between the minimum starting pressure ratio and the minimum operating pressure ratio.

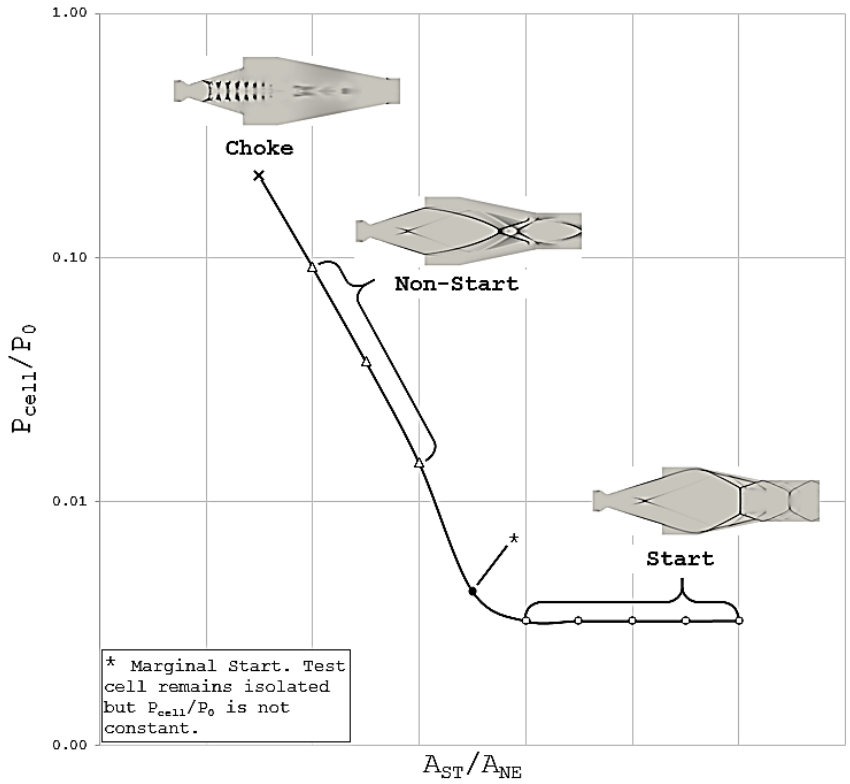

Fig. 3 – Mode of Operation and Shock Structure vs. P_{cell} and A_{ST}/A_{NE}

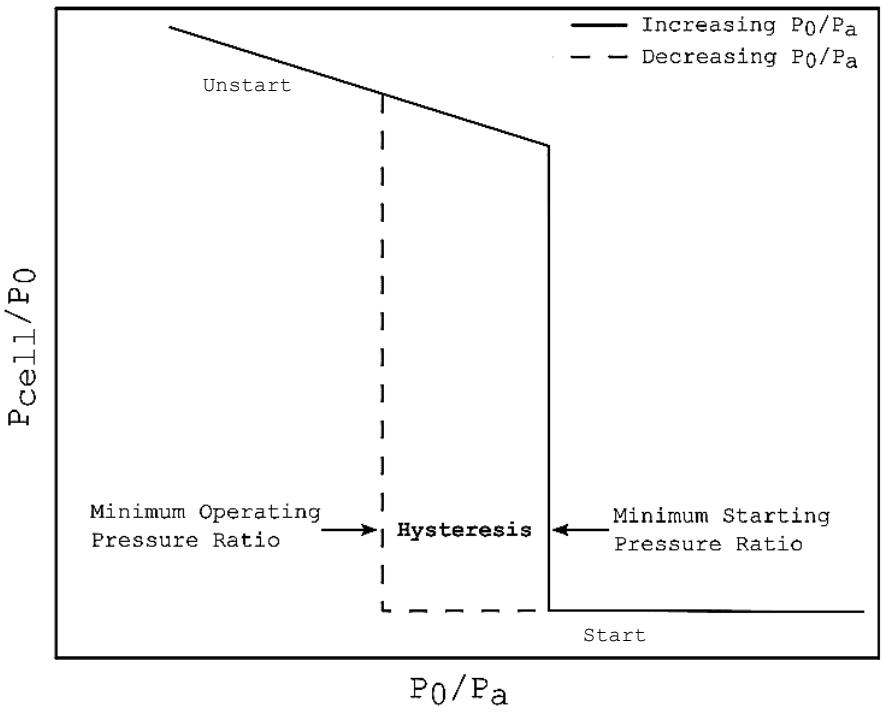

Fig. 4 – Typical Second Throat Diffuser Start/Unstart Behavior

Parameters Influencing Minimum Second Throat Size

Among the reasons diffuser design remains largely based on empirical data rather than theoretical models is the fact that there are numerous variables affecting their behavior. Below is a non-exhaustive list of parameters that influence the minimum size of the second throat.

- **P_0/P_a:** The ratio of stagnation pressure to ambient pressure is perhaps the most influential of all design parameters. Given a fixed nozzle geometry, it is the most basal reason a diffuser is being used in the first place – to prevent separation at the nozzle lip due to a low P_{NE}/P_a. Though it does not solely predict a diffuser's ability to start, it is critical that this pressure is high enough to overcome the losses incurred in the diffuser and maintain supersonic flow.
- **T_0:** Stagnation temperature affects the thermodynamic properties of the working gas. Combined with a low P_0 and high A_{DI}/A_{NT}, a low T_0 can cause phase change to occur and drastically alter the internal diffuser flow.
- **γ:** The influence of the ratio of specific heats on diffuser operation is substantial due to its prominence in the fundamental compressible flow equations. From Mach number to shock losses, γ influences nearly every aspect of the internal flow field.
- **θ_{NE}:** The nozzle exit angle largely determines the intensity of the plume's impingement on the diffuser inlet when the start condition is reached. Therefore, it directly impacts the shock-induced P_0 losses. Because the local P_0 in the second throat ultimately determines whether the diffuser can pass the mass flow of the rocket, this parameter can have a large impact on minimum A_{ST}.
- **A_{DI}/A_{NE}:** The diffuser inlet to nozzle exit area ratio controls the plume's maximum Mach number and affects its impingement location and resultant oblique shock strength. This combination can have a strong impact on both P_0 losses and the overall diffuser shock structure.
- **L_{DI}:** The length of the diffuser inlet influences minimum A_{ST} in two ways. First, it directly affects whether the plume impingement occurs within the inlet or contraction, establishing a flow field with either one or two oblique shocks. Second, assuming the diffuser is well-designed and impingement occurs in the inlet, it alters the interaction of the two oblique shocks generated by plume impingement and diffuser contraction.

- **θ_{DC}:** The angle of the diffuser contraction determines the strength of the contraction-induced oblique shock and consequently its P_0 losses and β.
- **L_{ST}:** The length of the second throat can contribute to P_0 losses by providing more or less space for oblique shock reflections to occur before exiting the diffuser. Viscous P_0 losses also occur, but are relatively small.
- **Physical Scale:** Boundary layer thickness is exaggerated at a small physical scale compared to a proportional geometry at a larger physical scale. This effectively reduces the cross-sectional area seen by the inviscid core flow and increases the minimum second throat area.
- **Chemical Reactions:** Reacting flow changes the fundamental thermodynamic properties of the working gas while it moves throughout the diffuser and can make theoretical analysis of diffusers exceedingly difficult.
- **Secondary Flows:** Any secondary purge or inertion flow adds mass into the system and increases the minimum second throat size. This effect is dependent on the fluid being introduced and its injection geometry, pressure, temperature, and mass flow rate.
- **Diffuser Cooling:** Cooling the inner wall of the diffuser to prevent damage decreases the temperature of the boundary layer and reduces its thickness. The decreased thickness of the boundary layer effectively increases the cross-sectional area seen by the inviscid core flow and decreases the minimum size of the second throat. This effect is very small compared to the effects of the other variables on this list.

Legacy Determinations of Minimum Second Throat Size

American rocket engineers began experiencing problems with boundary layer separation during engine tests as early as 1945, due to increased interest in high nozzle expansion ratios [1]. One of the methods employed to overcome this obstacle was to apply the principles of supersonic wind tunnels to design diffusers that simulated the low pressure of an altitude environment at the nozzle lip. To the author’s knowledge, the earliest report that addresses the limitation on the second throat area of such diffusers is a World War II era NACA Report entitled “Preliminary

Investigation of Supersonic Diffusers", published in 1945 [2]. The calculation of minimum second throat area is performed under the assumption that the diffuser must allow a normal shock to pass through it without any mass accumulation during the transient startup process. Normal shock losses are greatest at the highest Mach number conditions within the flow. This occurs when the plume expands to the diffuser's maximum area. The quasi-one-dimensional isentropic Mach number is found at that point by solving equation (1) and used to compute a new Mach number and P_0 downstream of the shock with equations (2) and (3). The new, reduced P_0 is now responsible for driving the same mass flow rate through the second throat, and can be used directly to determine its minimum size. Because mass flow per unit area is maximized at Mach 1, this condition is used in the isentropic mass flux relation to produce equation (4). All fundamental compressible flow equations used in this method are rearranged forms of those found in NACA Report 1135 [3].

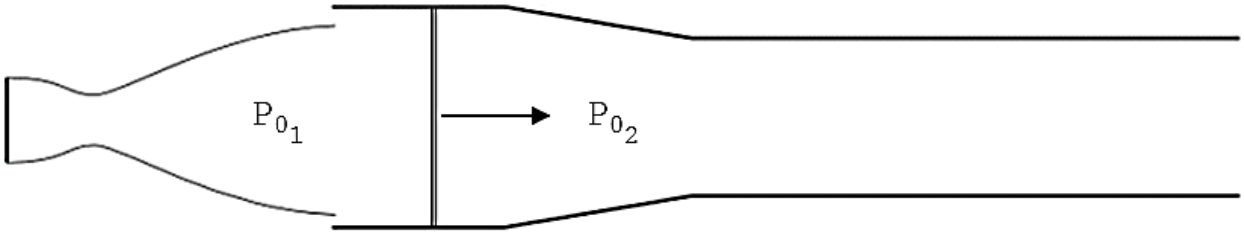

Fig. 5 – Basic Illustration of Normal Shock Method

$$\frac{A_{DI}}{A_{NT}} = \frac{1}{M_{DI}}\left(\frac{1+\frac{\gamma-1}{2}M_{DI}^2}{\frac{\gamma+1}{2}}\right)^{\frac{\gamma+1}{2(\gamma-1)}} \tag{1}$$

$$M_2 = \sqrt{\frac{1+\frac{\gamma-1}{2}M_{DI}^2}{\gamma M_{DI}^2 - \frac{\gamma-1}{2}}} \tag{2}$$

$$P_{0_2} = P_{0_1}\left[\frac{\frac{\gamma+1}{2}M_{DI}^2}{1+\frac{\gamma-1}{2}M_{DI}^2}\right]^{\frac{\gamma}{\gamma-1}}\left[\frac{1}{\frac{2\gamma}{\gamma+1}M_{DI}^2 - \frac{\gamma-1}{\gamma+1}}\right]^{\frac{1}{\gamma-1}} \tag{3}$$

$$A_{ST_{min}} = \dot{m}\left[P_{0_2}\sqrt{\frac{\gamma}{RT_0}}\left(1+\frac{\gamma-1}{2}\right)^{\frac{\gamma+1}{2(1-\gamma)}}\right]^{-1} \tag{4}$$

Because a normal shock at the diffuser inlet represents the greatest possible shock-induced stagnation pressure loss through a diffuser, it consistently produces high estimates of minimum second throat size. The fact that it is reliably conservative and easy to use has made it very popular for the last fifty years. However, a significant drawback to computing the second throat area in such a manner is that it does not provide a performance-optimized design. The system of oblique shocks that actually exists within a diffuser is heavily dependent on the specific geometric configuration and can produce a substantially lower cumulative P_0 loss than a normal shock. In turn, that allows most real diffusers to start with much tighter throats and against a higher back pressure than one designed using the normal shock method. Recognizing this, Wegener and Lobb of the U.S. Naval Ordinance Laboratory [4] combined data from several supersonic and hypersonic wind tunnels in 1952 to create an experimental curve fit of minimum starting throat area (Fig. 6). They noted that the normal shock method produces a minimum throat size that is up to twice as large as the experimentally determined value.

In the late 1950s, NASA began examining diffusers explicitly for simulated altitude testing of high expansion ratio rocket engines that would incur boundary layer separation if fired at sea level conditions. Lewis Research Center conducted an experimental study of second throat diffusers using gaseous nitrogen as the working fluid [5]. It added the Navy's data set to its own, and produced a curve-fit from a diverse array of data (Fig. 7). Configurations included conical and contoured nozzles, two-dimensional and three-dimensional geometries, cold flow tests with air and nitrogen, and a hot-fire engine. It should be noted that each data set contributing to this curve fit occupied its own space in the Mach number vs. contraction ratio domain, and it was not confirmed that the disparate configurations would have produced the same results at similar flow conditions. Also of note is that this reference considered the contraction ratio to be A_{DI}/A_{ST} rather than A_{ST}/A_{DI}.

From 1961-1968, the Arnold Engineering Development Center (AEDC) conducted an extensive experimental study to assess the sensitivity of diffuser performance to various design parameters. In addition, a new theoretical method of calculating minimum throat size was described for both short and long second throat diffusers. It employed a force balance

between the nozzle exit and second throat exit and accounted for nozzle thrust, the pressure force in the test cell, the pressure force on the contraction ramp after an oblique shock produced by a turning angle of 35° (fixed assumption, not calculated based on geometry), the dynamic pressure force at the second throat, and the friction force through the second throat. The results of the force balance method were compared to normal shock theory and the NASA empirical curve fit, as shown in Fig. 8. Additional information can be found in references [6-8].

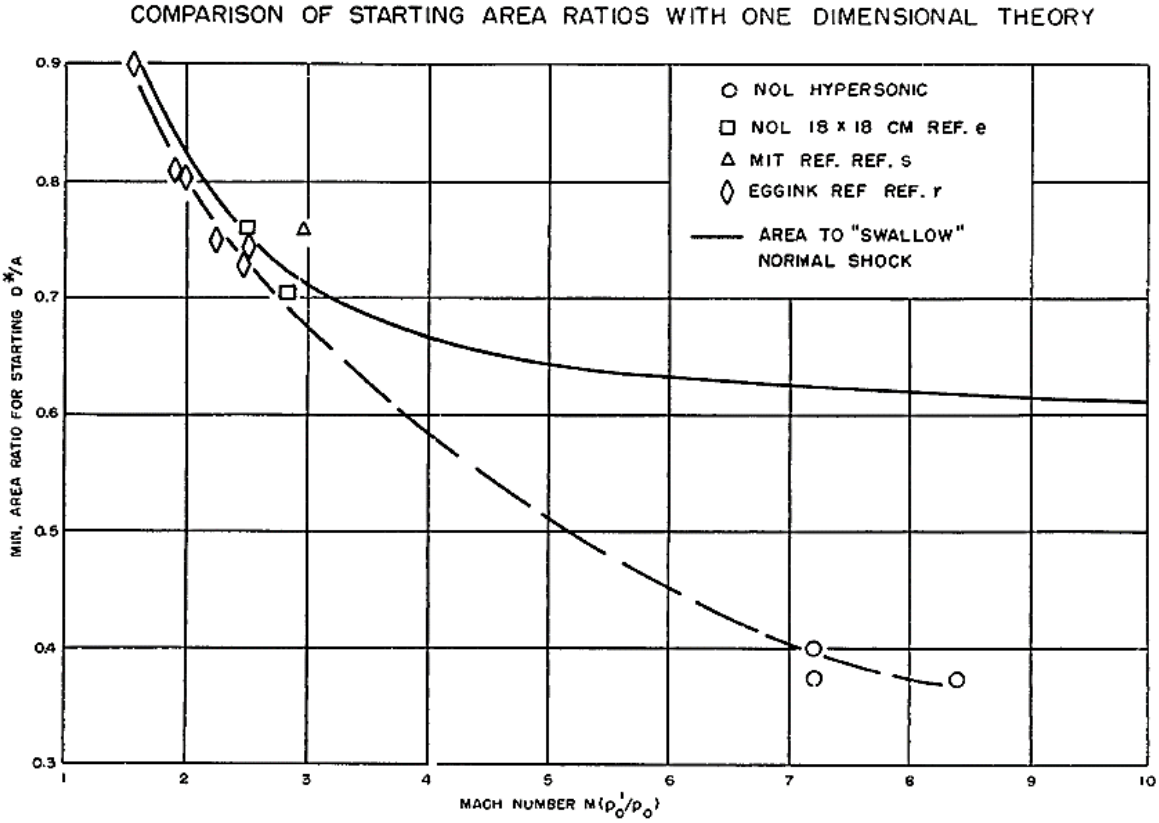

Fig. 6 – Experimental and Normal Shock Curves from [4]

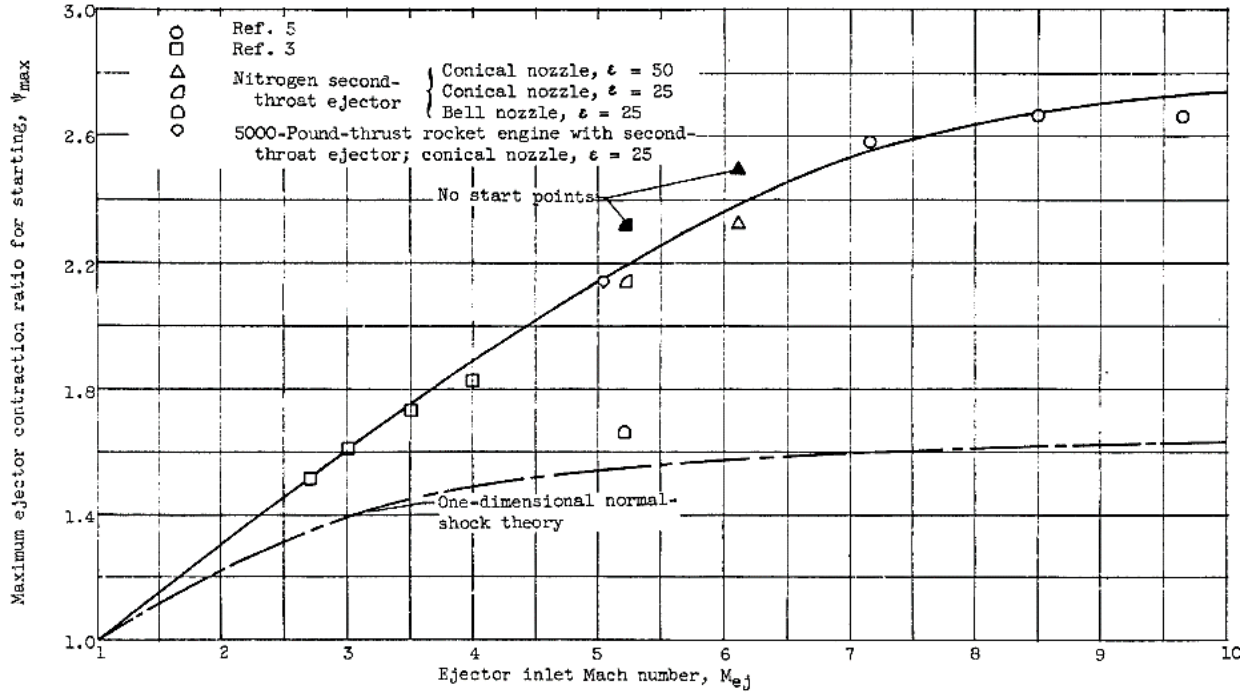

Fig. 7 – Experimental and Normal Shock Curves from [5]

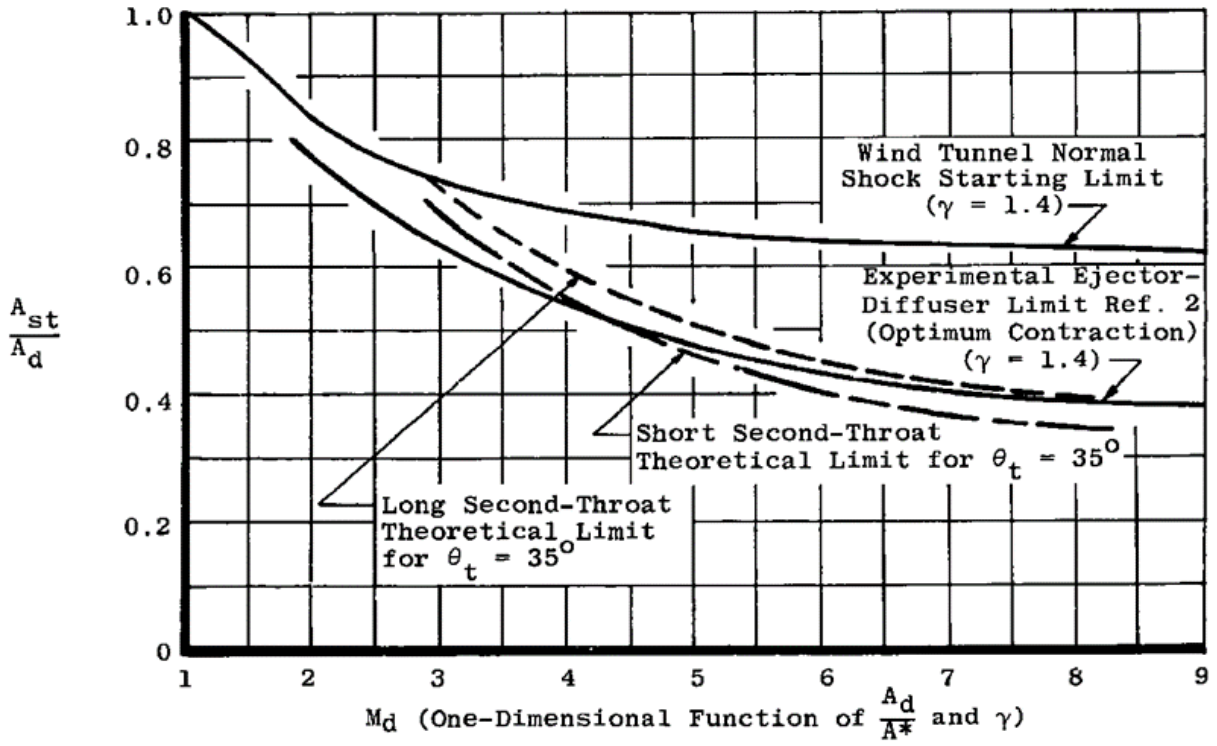

Fig. 8 – Theoretical and Experimental Curves from [7]

COMPUTATIONAL FLUID DYNAMICS STUDY

Despite the improvements to theoretical analysis made by AEDC, the applicability of the force balance method for determining minimum second throat is limited to a small subset of diffuser geometries. The assumption of a 35° total turning angle represents a configuration with high θ_{NE}, θ_{DC}, and A_{DI}/A_{NE}. The author of this paper attempted to extend the utility of the method by applying the turning angle equation used by AEDC in [7] for its pumping performance calculations. Unfortunately, this resulted in unphysical second throat areas for geometries with a total turning angle below ~30° for γ = 1.4. Lower values of γ exacerbated the problem. In order to analyze the second throat limitations for a wide range of diffuser configurations, a new theoretical model needed to be developed. As such, a better understanding of diffusers' internal flow structure was desired. The number of hardware configurations required was considered to make experimental examination unwieldy and prohibitively costly. Computational simulation offered the same potential insight into diffuser flows at significantly reduced cost and was selected for this investigation.

The primary objective of this computational endeavor was to understand the variance of minimum second throat size with respect to A_{NE}/A_{NT}, A_{DI}/A_{NE}, and γ. A set of geometries was established to cover the range of interest and the second throat area was varied to find the transition point between the diffuser start and non-start conditions. An overview of the configurations is given in Table 1. The A_{DI}/A_{NE} = 1.3 and 2.1 configurations used slightly different parameters in order for them to be representative of previously-tested hardware at NASA Stennis Space Center and AEDC [7], respectively. To eliminate the possibility of predicting a non-start caused by lack of driving pressure, P_0/P_a = 400 was specified. Physical scale was chosen to be close to that of the aforementioned tests, with all dimensions based on a fixed nozzle exit radius of 4.5 inches. All computational meshes were created with Pointwise grid generation software. A wall spacing of 0.00035 inches was used to provide adequate resolution in the boundary layer (y^+ <= 50) and a uniform axial spacing of 0.0035 inches within the diffuser to cap the cell aspect ratio at 10. A significantly larger and coarser mesh was used downstream of the diffuser to enforce the ambient pressure. The

cumulative cell count was on the order of 400,000 for all grids. A typical diffuser mesh is shown in Fig. 9.

A_{DI}/A_{NE}	A_{NE}/A_{NT}	θ_{NE}	$(L/D)_{DI}$	θ_{DC}	$(L/D)_{DT}$
1.3	20,50,90,110	15	0.44	6	2.75
1.5	10,50,90	15	0.5	6	2.75
1.7	10,50,90	15	0.5	6	2.75
1.9	10,50,90	15	0.5	6	2.75
2.1	12,50,90	18	0.5	12	8

Table 1 – Overview of Simulated Geometries

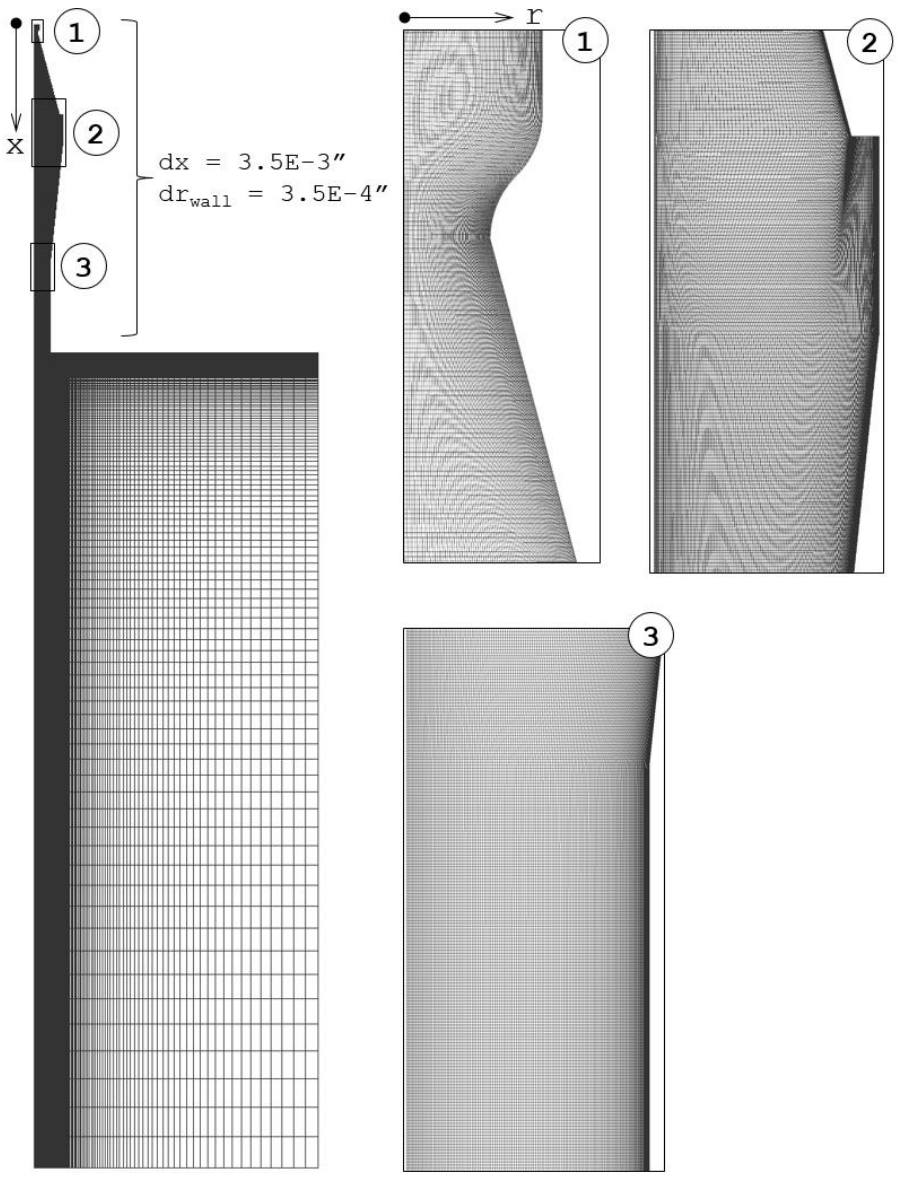

Fig. 9 – Example Diffuser Mesh

Loci/CHEM is a CFD code being developed by Mississippi State University with funding from multiple government agencies. Loci is a rule-based program control framework in which an application is described in terms of a collection of simple computational kernels [9]. CHEM is a second-order accurate, density-based flow solver built on the Loci framework. Key features of CHEM include multiple turbulence models, compressibility correction, inviscid flux limitation, finite-rate chemistry, real-fluid equations of state, Eulerian and Lagrangian multiphase models, support for generalized unstructured meshes, adaptive meshing, and automatic dynamic partitioning. A detailed description of theoretical and numerical formulation may be found in the Loci/CHEM User's manual [10].

CHEM has been used extensively by the CFD team at NASA Stennis and has been found to reliably predict diffuser flows, including boundary layer separation, shock structure, and pressure fields. An attempt to validate the code's ability to predict second-throat-driven start/non-start was made using the geometries and experimental data from [7] since it explicitly defined its criterion for start. Unfortunately, the CFD analyses indicated that the listed cases only produced pressure-driven non-start (insufficient P_0) rather than second-throat-driven non-start (insufficient A_{ST}). This was tested by running the pressure ratio above that listed in the experiments to see if the diffusers behaved differently. All started. The maximum P_0/P_a for the experiments was only 2.7, not exceedingly far above the value of 1.86 required just to have choked flow at the nozzle throat. It is the author's opinion that the pressure ratio across the system was insufficient to preclude the possibility of a pressure-driven non-start. No other known reference explicitly lists its geometry configurations, start criterion, and operating conditions. Therefore, the attempt to validate the CFD with experimental data was left for future work.

Standard solver inputs were applied to all cases (Table 2), with the exception of changes to the chemistry model to create perfect gases of $\gamma = 1.25$ and $\gamma = 1.4$. Each of the simulations ran on 300 processors on NASA's Pleiades supercomputer and completed the allotted number of iterations in about 3 hours.

Spatial Dimensionality:	2D Axisymmetric
Equation of State:	Perfect Gas
Spatial Discretization:	2nd Order
Temporal Discretization:	1st Order Implicit (Global time step)
Time Step:	5e-6 s
Iterations:	250,000
Turbulence Model:	Menter's Baseline
Compressibility Correction:	Wilcox
Boundary Layer Model:	Compressible Wall Functions
Chemical Reactions:	None
Phase Change:	None
Secondary Flow:	None
Initial Conditions:	P = 1 psia, T = 325 K, V = 0 m/s
Injector Inflow Conditions:	P_0 = 400 psia T_0 = 325 K Turbulence Intensity = 10%

Table 2 – Summary of Loci/CHEM Solver Settings

Two distinct diffuser flow patterns were observed at the start/non-start transition point. At low A_{DI}/A_{NE}, the plume expands out of the nozzle, impinges on the diffuser wall, and turns into itself along the contraction ramp. This produces a series of oblique shocks that intersect and create a natural point for a normal shock to rest. The flow re-accelerates to supersonic speeds through the second throat. This approximate pattern is shown in Fig. 10. At high A_{DI}/A_{NE}, the angle of the plume decreases with respect to the centerline, and the impingement occurs further downstream. Given a fixed $(L/D)_{DI}$, this means that the impingement can occur on the contraction ramp rather than the inlet. In turn, this only produces a single oblique shock, and a normal shock forms soon after that point. Again, the flow re-accelerates to supersonic speeds within the throat. Fig. 11 shows an example of this type of flow.

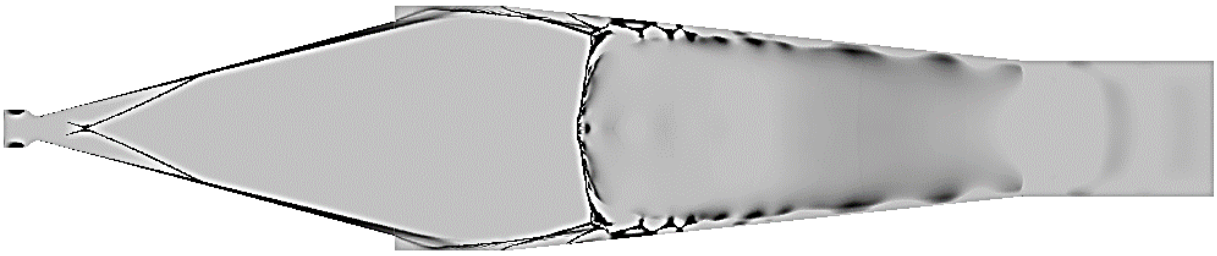

Fig. 10 – Start/Non-Start Diffuser Shock Structure at Low A_{DI}/A_{NE}

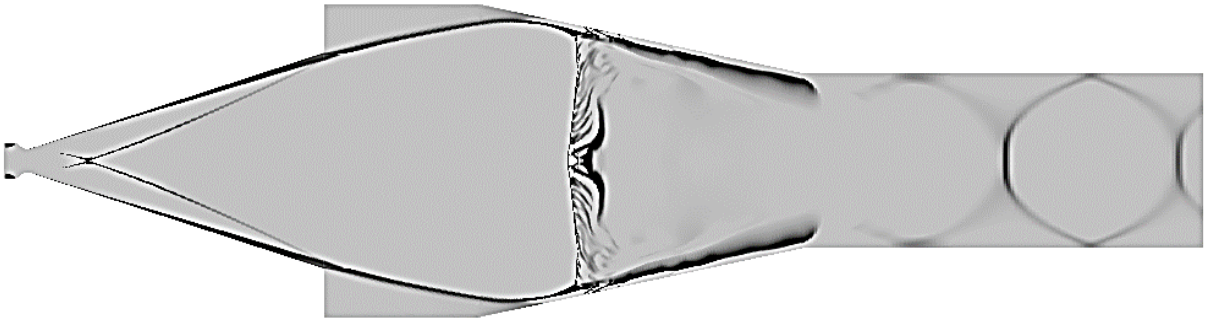

Fig. 11 – Start/Non-Start Diffuser Shock Structure at High A_{DI}/A_{NE}

After the two distinct sets of shock structures had been identified, an effort was made to reproduce the CFD results for minimum second throat area using quasi-one-dimensional compressible flow equations. The objective was to create a simple and effective model which could provide improved accuracy over historical methods and could be reproduced by anyone with a working knowledge of compressible flow. The following sections describe the development and combination of two models to provide a practical estimate of minimum second throat size. Detailed discussion of results for all methods is deferred until after each has been individually described.

THE WEIGHTED SHOCKS MODEL

The weighted shocks model was created in an attempt to approximate the flow field of diffusers with $A_{DI}/A_{NE} \leq 1.5$ at the minimum start condition. Accurate results in this region were of particular interest since lower A_{DI}/A_{NE} is typically associated with improved aerodynamic performance. Historical determinations of second throat size are also

very conservative since most diffusers were constructed with $A_{DI}/A_{NE} > 2$. The logic of this analysis is summarized following this paragraph. All requisite equations can be found in [3] unless otherwise specified, and are listed step-by-step in the appendix. As shown in Fig. 12, the structure of the computed weighted shocks flow field compares favorably to that produced by CFD. It should be noted that the CFD flow field was captured with a throat area slightly above the minimum. As a result, the normal shock is shock further downstream than would be expected for the true marginal start case. The geometric station labels used in the weighted shocks model are also found in the figure.

1. NT: Calculate the mass flow rate of the system with the isentropic mass flux equation applied at the nozzle throat.
2. NT to NE: Assume isentropic expansion through the nozzle to find the flow conditions at the nozzle exit.
3. NE to DI: Assume isentropic expansion to the diffuser inlet to find the minimum test cell pressure.
4. DI to IMP: Using the pressure obtained in the previous step, calculate the angle and location of the plume boundary as it expands to the diffuser inlet using the Newtonian method described by Henson and Robertson [11].
5. DI to OS1: Calculate the conditions behind the impingement-induced oblique shock and its angle (β) using the diffuser inlet conditions and the angle of the plume boundary as it reaches the diffuser wall.
6. OS1 to OS2: Use the flow conditions found in the previous step to calculate the conditions behind the contraction-induced oblique shock and its β.
7. INT: Find the geometric point of intersection of the impingement and contraction oblique shocks.
8. DI to NS: Assume a normal shock occupies the area between the two intersection points. Calculate mass flow rate through and P_0 behind the shock using diffuser inlet conditions.
9. Subtract the mass flow through the normal shock from the system mass flow rate. Scale the P_0 of OS2 to give the resultant mass flow through the area between the shock intersection point and the diffuser wall. This forces conservation of mass. Make sure to correct the mass flow for the difference in the area normal and flow path along the wall.

10. OS2 & NS to ST: Apply an area-based weighted average of the two P_0 values to produce an estimate of the P_0 experienced at the inlet of the second throat.
11. Determine the minimum second throat size based on the weighted P_0 using the isentropic mass flux equation.

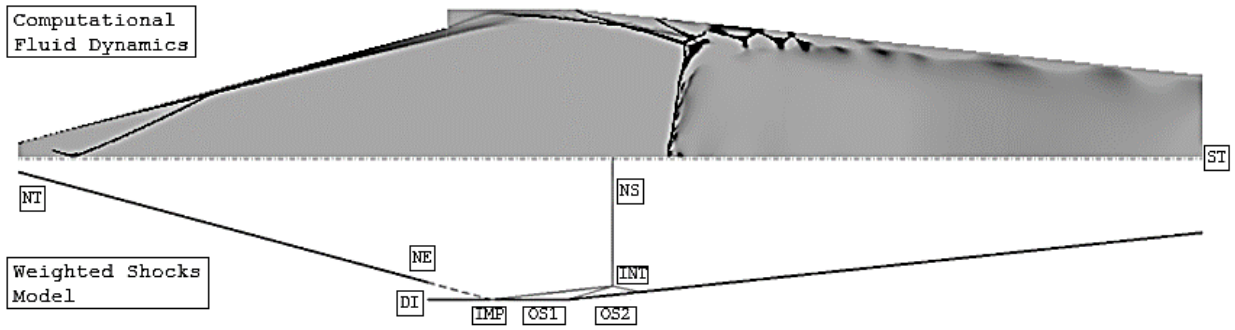

Fig. 12 – Comparison of CFD and Weighted Shocks Flow Fields

THE ISENTROPIC COMPRESSION MODEL

As displayed in Fig. 11, the flow fields of diffusers with $A_{DI}/A_{NE} \geq 1.7$ have a very different structure compared to that assumed by the weighted shocks model. This is primarily driven by the occurrence of impingement on the conical contraction rather than the cylindrical inlet. The structure is defined by a stronger, single oblique shock which almost immediately results in flow separation and a normal shock. To approximate this flow field, it is assumed that the flow undergoes isentropic compression as it is turned from the average half-angle at nozzle exit to axial flow through a normal shock. Fig. 13 shows the CFD-produced flow field and calculation locations for this model. The logic is summarized below, with full equations listed in the appendix.

1. NT: Calculate the mass flow rate of the system with the isentropic mass flux equation applied at the nozzle throat.
2. NT to NE: Assume isentropic expansion through the nozzle to find the flow conditions at the nozzle exit.
3. NE to NS1: Assume isentropic compression from the average flow half-angle to axial flow right before the normal shock. Use an inverse

Prandtl-Meyer expansion to find the Mach number after the turn and the isentropic relations to define the resultant flow conditions.

4. NS1 to NS2: Pass the isentropically-compressed flow through a normal shock and find the post-shock P_0.
5. NS2 to ST: Determine the second throat size based on the post-shock P_0 and system mass flow rate.

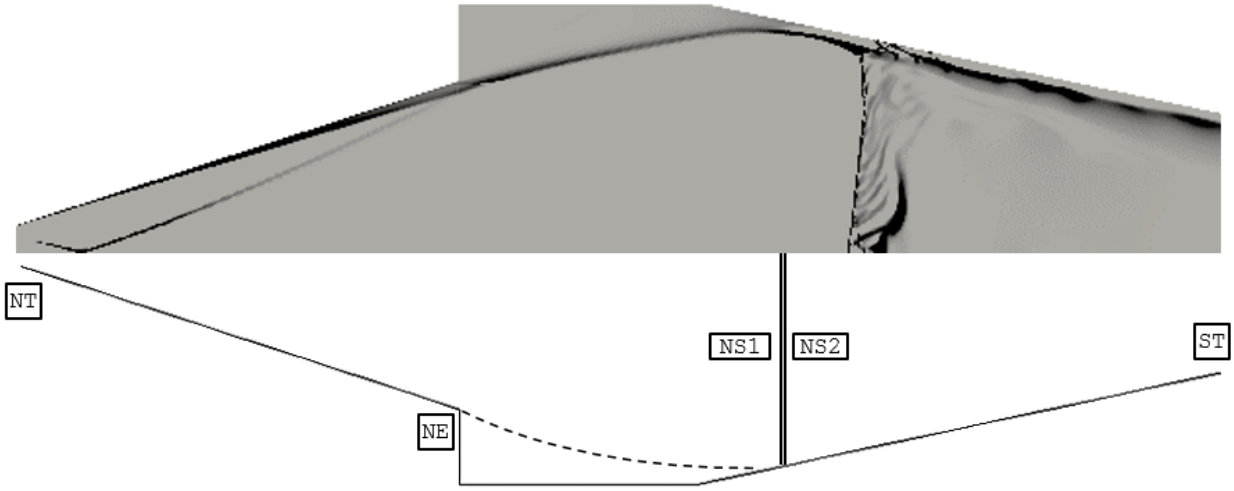

Fig. 13 – Comparison of CFD and Isentropic Compression Flow Fields

THE 3-ZONE METHOD

The 3-zone method is a simple combination of the weighted shocks and isentropic compression models to account for the transitional region of A_{DI}/A_{NE} in which the flow field is somewhere between the two assumed. The 3-zone method can be summarized as follows:

1. Zone 1: $1.3 \leq A_{DI}/A_{NE} < 1.5$. Use the weighted shocks model.
2. Zone 2: $1.5 \leq A_{DI}/A_{NE} \leq 1.7$. Calculate the results of both the weighted shock and isentropic compression models. Use the lower of the two.
3. Zone 3: $1.7 < A_{DI}/A_{NE} \leq 2.1$. Use the isentropic compression model.
4. Apply an application-appropriate margin for design.

DISCUSSION OF RESULTS

Comparison of CFD Results to Legacy Methods

Results of the CFD study were plotted in the contraction ratio vs. Mach number framework for comparison to historical determinations of minimum throat size for a working fluid of γ = 1.4 (Fig. 14). The CFD indicates consistently lower minimum throat areas compared to previous studies. This is believed to be an artifact of the framework in which the results have been presented. It is important to note the scatter in the computational values when plotted this way. Scatter in experimental data is inevitable (especially given data from multiple sources and configurations, as in Refs. [4-8]) and can easily be explained away as measurement uncertainty or suppressed with a curve fit. However, CFD results performed with the exact same solver settings and flow conditions should be entirely self-consistent, so the scatter was considered justification for re-evaluation of both the legacy data and the way in which it has been interpreted.

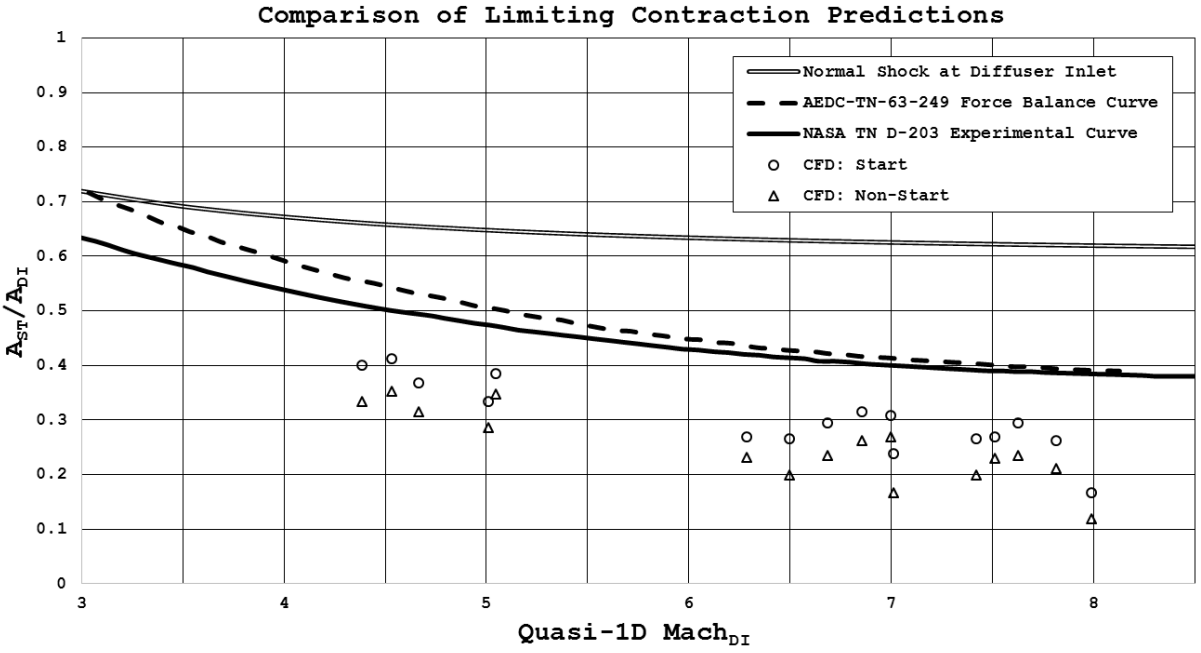

Fig. 14 – Loci/CHEM Predictions vs. Historical Methods, γ = 1.4

In all previous studies, minimum second throat area was viewed in a diffuser-oriented geometry/flow framework which presented the physical

limitation as a restriction on the diffuser contraction ratio that varied with Mach number. This frame of reference has been widely used and is a natural product of the normal shock method, where the diffuser inlet Mach number is the primary input. Nevertheless, it has two significant drawbacks. The first is an assumption that the variance of contraction ratio (A_{ST}/A_{DI}) is solely a function of the diffuser Mach number. The true limitation is on the ratio of the second throat to the first (A_{ST}/A_{NT}), driven by all losses that occur between the two. This becomes apparent when the contraction ratio is presented as a function of the throat-to-throat ratio and upstream area ratios, as in equation (5).

$$\frac{A_{ST}}{A_{DI}} = \frac{\frac{A_{ST}}{A_{NT}}}{\frac{A_{NE}}{A_{NT}}\frac{A_{DI}}{A_{NE}}} \tag{5}$$

It is true that A_{NE}/A_{NT} does not impact the flow field apart from the Mach number it generates because expansion through the nozzle is isentropic. However, A_{DI}/A_{NE} affects the angle and location of impingement in addition to the Mach number, which can substantially affect the shock structure and associated P_0 losses. The effects of θ_{NE} and θ_{DC} are also overlooked by the contraction ratio vs. Mach framework, contributing to additional scatter in the results. The second drawback of the historical perspective is the assumption that the quasi-one-dimensional diffuser Mach number is always representative of the flow. This would be true if the plume were guaranteed to expand to the diffuser inlet for all cases. In reality, it is possible for the plume to expand less aggressively and for impingement to occur on the contraction ramp rather than the maximum area. The result is a decoupling of the true flow from the assumed flow which renders the geometric contraction ratio meaningless. This effect is of particular concern for combinations of high A_{DI}/A_{NE} and low $(L/D)_{DI}$.

To address some of these issues, a new nozzle-based, geometry-only framework was selected to represent the second throat restriction. A_{ST}/A_{NE} is plotted against A_{NE}/A_{NT}. This frame of reference only makes the assumption that the nozzle is flowing full so that the expansion ratio is representative of the flow. This will always be the case for diffusers reaching the start condition. Nozzle exit was chosen to normalize the second throat area rather than the nozzle throat because it is the parameter that ultimately dictates physical scale and establishes the static pressure ratio across the diffuser. This perspective does not

collapse the data as well as the historical framework, but it is the author's opinion that it presents the same information much more accurately despite the fact that it still fails to capture the effect of other key variables like θ_{NE}. Unfortunately, the historical methods/data cannot be translated into this framework without further assumptions. As such, only the CFD results and 3-zone model are shown this way in the following sections.

Comparison of CFD Results to the 3-Zone Method

The variations of CFD-produced flow regime with γ and A_{DI}/A_{NE} are shown within the new nozzle-based frame of reference in Fig. 15. Distinctions are made between the start, non-start, and choke conditions. In the interest of clarity, only the CFD cases which bounded a change between these flow regimes were plotted. Minimum second throat areas produced by the normal shock, isentropic compression, and weighted shock methods are also displayed. As expected, the normal shock method is by far the most conservative prediction. For γ = 1.4, the weighted shocks model produces the best approximation of the CFD results if $A_{DI}/A_{NE} \leq 1.5$ but begins to exaggerate the Mach number passing through the normal shock and becomes more conservative beyond that. The isentropic compression model has the opposite trend in error. It fails to account for the relatively-lower oblique shock losses that occur for $A_{DI}/A_{NE} \leq 1.5$ and over-predicts the minimum area, but becomes more representative of the flow beyond that. Thus for γ = 1.4, the optimum transition/crossover point for the 3-zone method was $A_{DI}/A_{NE} = 1.5$. All predictions of minimum second throat areas were lower at γ=1.25, and the optimum transition point between weighted shocks and isentropic compression shifts to $A_{DI}/A_{NE} = 1.7$. This variance in transition point was the motivation for selecting a 3-zone method rather than a 2-zone approach with a single point of crossover between the models.

Figs. 16 & 17 display the same predictions as Fig. 15, filtered through the 3-zone method. The results were plotted with the objective of comparing the conservatism of the 3-zone method to that of the normal shock method using the CFD results as a baseline in lieu of suitable data. As such, all values greater than one indicate a conservative estimate. The CFD minimum starting second throat area was taken to be the average between the minimum simulated area producing start and the

maximum simulated area producing non-start. Points lying above the solid horizontal lines predict minimum starting second throat areas larger than that produced by CFD. Conversely, those below the line predict a lower minimum area. The ratio plotted on the vertical axis is effectively the safety factor of the theoretical models compared to the CFD. The averages and standard deviations of the models' safety factors are given in Table 3.

Overall, the 3-zone method produced results much closer to the CFD than the normal shock model with conservatism reduced by an average of 52%. However, it does under-predict the minimum second throat size by up to 10% for some cases where $A_{NE}/A_{NT} < 20$ and $A_{DI}/A_{NE} \geq 1.7$. This inaccuracy was restricted to the isentropic compression model and was more common at γ=1.4.

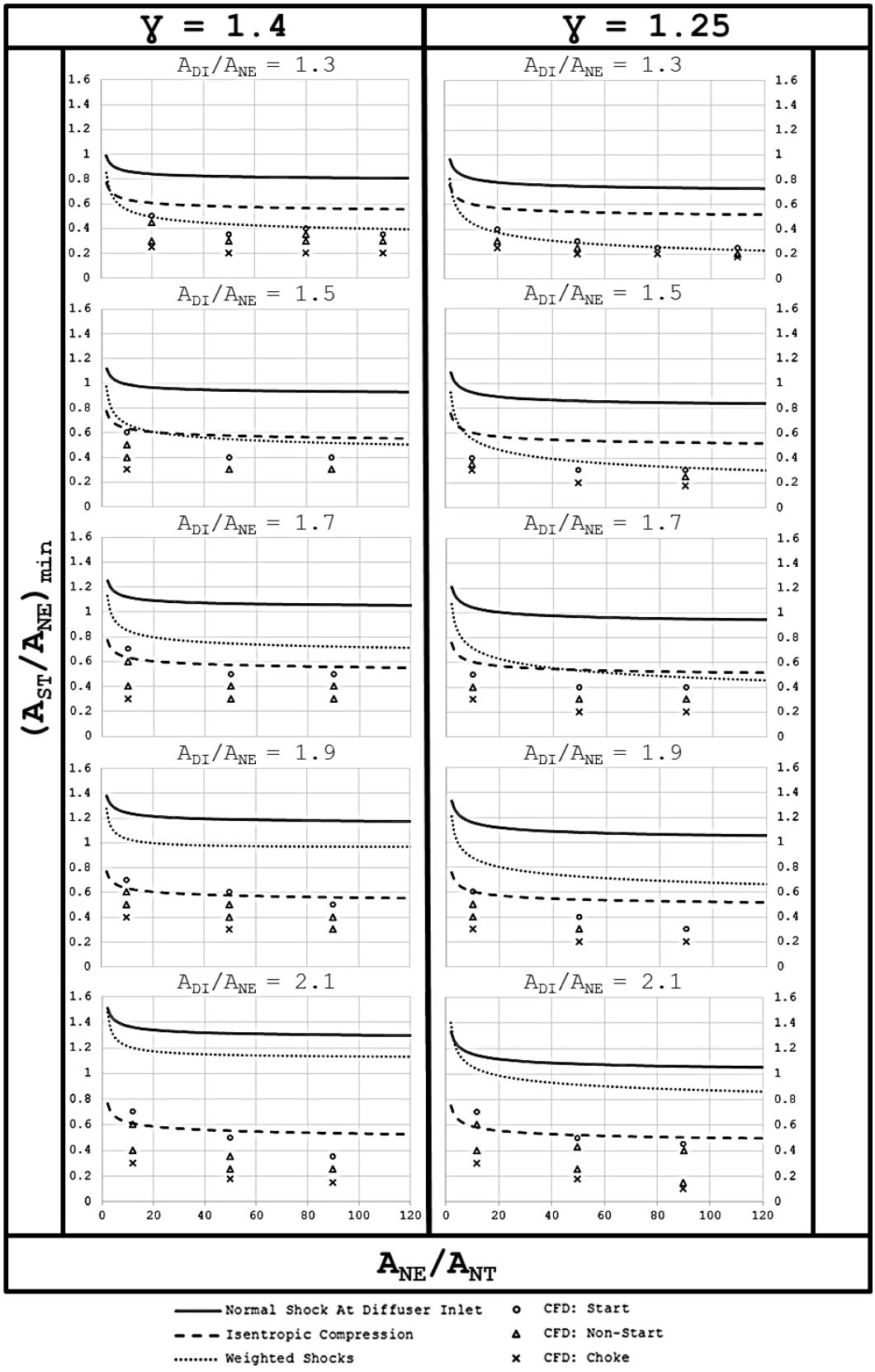

Fig. 15 – Comparison of Theoretical and CFD Results

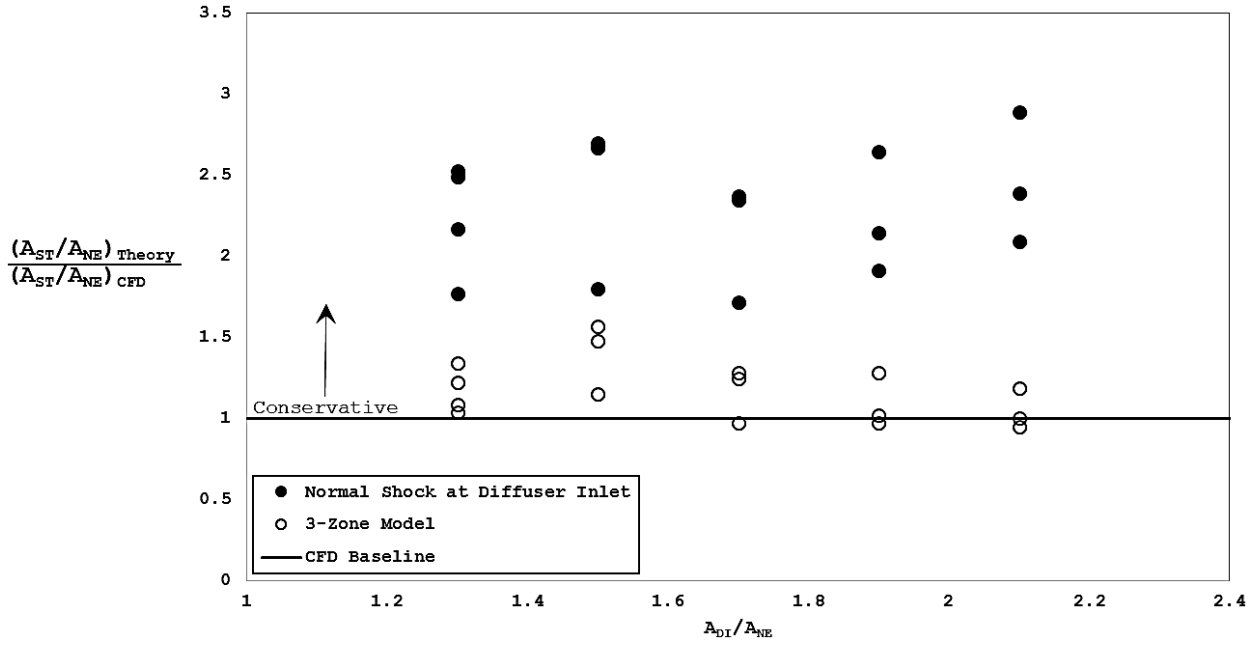

Fig. 16 – Relative Conservatism of 3-Zone and Normal Shock Methods, Normalized by CFD Results, γ = 1.4

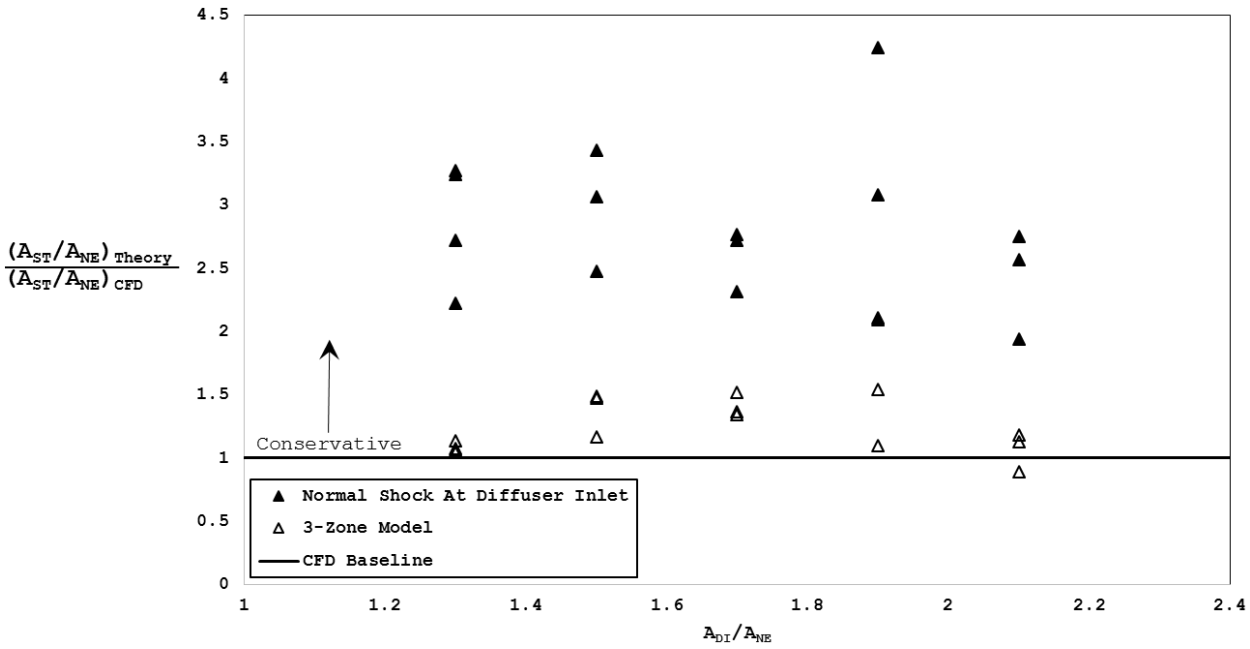

Fig. 17 – Relative Conservatism of 3-Zone and Normal Shock Methods, Normalized by CFD Results, γ = 1.25

		3-Zone	NS
γ = 1.25	Avg.	1.29	2.81
	Std. Dev.	0.28	0.56
γ = 1.4	Avg.	1.18	2.29
	Std. Dev.	0.18	0.35

Table 3 – Statistical Comparison of Theoretical Safety Factors

CONCLUSIONS

In this report, the results of a CFD investigation of minimum diffuser second throat area have been presented in both diffuser-oriented and nozzle-oriented frames of reference. Two distinct internal diffuser flow fields were observed, and two quasi-one-dimensional compressible flow models approximating their individual shock structures were described. The two models were incorporated into a 3-zone method for predicting minimum second throat area which compared favorably with CFD and produced less-conservative estimates than historical methods. Suitable data on second-throat-induced diffuser non-start was not found upon review of available literature. All known references that addressed the second throat limitation either failed to provide explicit geometries or tested at P_0/P_a values too low to rule out pressure-induced non-start. As such, validation has been left for future work.

REFERENCES

[1] Sutton, G., "History of Liquid Propellant Rocket Engines," *Technology and Hardware*, 1st ed., AIAA, New York, 2006, pp. 33-240.

[2] Kantrowitz, A., and Donaldson, C., "Preliminary Investigation of Supersonic Diffusers," NACA ACR No. L5D20, May 1945.

[3] "Equations, Tables, and Charts for Compressible Flow," NACA Report 1135, 1953.

[4] Wegener, P., and Lobb, R., "NOL Hypersonic Tunnel No. 4 Results II: Diffuser Investigation," NAVORD Report 2376, May 1952.

[5] Jones, W., Price, H., and Lorenzo, C., “Experimental Study of Zero-Flow Ejectors Using Gaseous Nitrogen,” NASA TN D-203, March 1960.

[6] Bauer, R., and German, R., “The Effect of Second Throat Geometry on the Performance of Ejectors Without Induced Flow,” AEDC-TDR-61-133, November 1961.

[7] Panesci, J., and German, R., “An Analysis of Second-Throat Diffuser Performance for Zero-Secondary-Flow Ejector Systems,” AEDC-TDR-63-249, December 1963.

[8] Taylor, D., and Toline, F., “Summary of Exhaust Gas Ejector-Diffuser Research,” AEDC-TDR-68-84, October 1968.

[9] Luke, E., and George, T., "Loci: A Rule-Based Framework for Parallel Multidisciplinary Simulation Synthesis," Journal of Functional Programming, Volume 15, Issue 03, 2005, pp. 477-502, Cambridge University Press.

[10] Luke, E., Tong, X., Wu, J., Cinnella, P., and Chamberlain, R., “CHEM 3.3: A Finite-Rate Viscous Chemistry Solver - The User Guide,” January 2013.

[11] Henson, J., and Robertson, J., “Methods of Approximating Inviscid Jet Boundaries for Highly Underexpanded Supersonic Nozzles,” AEDC-TDR-62-7, May 1962.

APPENDIX: STEP-BY-STEP CALCULATION PROCEDURE

The Weighted Shocks Model

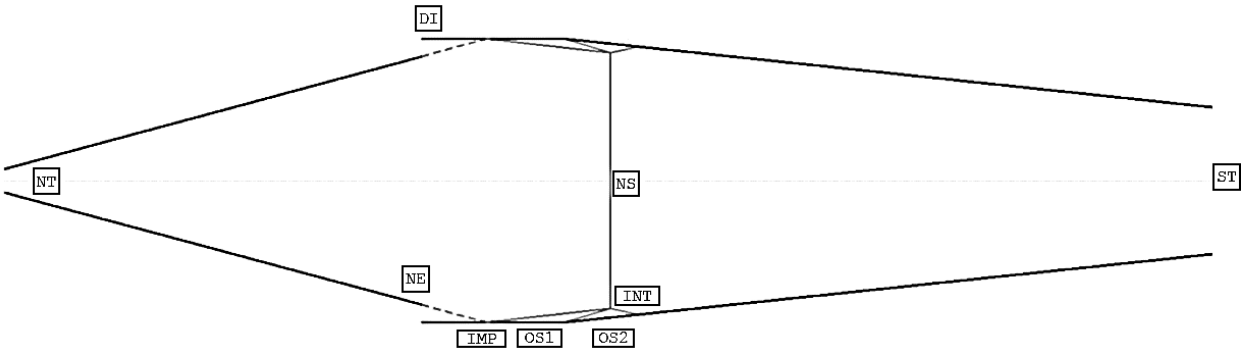

Fig. A1 – Calculation Locations for the Weighted Shocks Model

0. Requisite information: γ, P_0, T_0, A_{NT}, $\frac{A_{NE}}{A_{NT}}$, θ_{NE}, $\frac{A_{DI}}{A_{NE}}$, $\left(\frac{L}{D}\right)_{DI}$, θ_{DC}

1. NT: Calculate the mass flow rate of the system with the isentropic mass flux equation applied at the nozzle throat.

$$\dot{m}_{system} = (P_0 A)_{NT} \sqrt{\frac{\gamma}{RT_0}} \left(1+\frac{\gamma-1}{2}\right)^{\frac{\gamma+1}{2(1-\gamma)}} \tag{A1}$$

2. NT to NE: Assume isentropic expansion through the nozzle to find the flow conditions at the nozzle exit. Solve (A3) implicitly for M_{NE}.

$$P_{0_{NE}} = P_{0_{NT}} \tag{A2}$$

$$\frac{A_{NE}}{A_{NT}} = \left(\frac{1}{M_{NE}}\right)\left(\frac{1+\frac{\gamma-1}{2}M_{NE}^2}{\frac{\gamma+1}{2}}\right)^{\frac{\gamma+1}{2(\gamma-1)}} \tag{A3}$$

$$P_{NE} = \frac{P_{0_{NE}}}{\left(1+\frac{\gamma-1}{2}M_{NE}^2\right)^{\frac{\gamma}{\gamma-1}}} \tag{A4}$$

3. NE to DI: Assume isentropic expansion to the diffuser inlet to find the minimum test cell pressure. Solve (A6) implicitly for M_{DI}.

$$P_{0_{DI}} = P_{0_{NT}} \tag{A5}$$

$$\frac{A_{DI}}{A_{NT}} = \left(\frac{1}{M_{DI}}\right)\left(\frac{1+\frac{\gamma-1}{2}M_{DI}^2}{\frac{\gamma+1}{2}}\right)^{\frac{\gamma+1}{2(\gamma-1)}} \tag{A6}$$

$$P_{DI} = \frac{P_{0_{DI}}}{\left(1+\frac{\gamma-1}{2}M_{DI}{}^2\right)^{\frac{\gamma}{\gamma-1}}} \tag{A7}$$

4. DI to IMP: Using the pressure obtained in the previous step, calculate the angle and location of the plume boundary as it expands to the diffuser inlet using the Newtonian method described by Henson and Robertson [11].

$$r_{NT} = \sqrt{\frac{A_{NT}}{\pi}} \tag{A8}$$

$$r_{NE} = r_{NT}\sqrt{\frac{A_{NE}}{A_{NT}}} \tag{A9}$$

$$r_{DI} = r_{NE}\sqrt{\frac{A_{DI}}{A_{NE}}} \tag{A10}$$

$$\nu_{NE} = \sqrt{\frac{\gamma+1}{\gamma-1}}\tan^{-1}\sqrt{\frac{\gamma-1}{\gamma+1}(M_{NE}^2-1)} - \tan^{-1}\sqrt{M_{NE}^2-1} \tag{A11}$$

$$\nu_{DI} = \sqrt{\frac{\gamma+1}{\gamma-1}}\tan^{-1}\sqrt{\frac{\gamma-1}{\gamma+1}(M_{DI}^2-1)} - \tan^{-1}\sqrt{M_{DI}^2-1} \tag{A12}$$

$$\alpha_1 = \nu_{DI} - \nu_{NE} + \theta_{NE} \tag{A13}$$

$$r_1 = r_{NE} \tag{A14}$$

$$x_1 = x_{NE} \tag{A15}$$

While $r_i \leq r_{DI}$:

$$r_i = r_{NE} + (i-1)\,dr \qquad i=1,2,3\ldots \tag{A16}$$

$$\frac{A_i}{A_{NT}} = \left(\frac{r_i}{r_{NE}}\right)^2 \left(\frac{A_{DI}}{A_{NT}}\right) \qquad i=1,2,3\ldots \tag{A17}$$

Note that A_DI is used as the effective area ratio experienced by the plume boundary at the nozzle lip because the boundary is assumed to experience Prandtl-Meyer expansion to the test cell pressure at that location. This is used as the initial condition for iteration.

$$\frac{A_i}{A_{NT}} = \left(\frac{1}{M_i}\right)\left(\frac{1+\frac{\gamma-1}{2}M_i^2}{\frac{\gamma+1}{2}}\right)^{\frac{\gamma+1}{2(\gamma-1)}} \quad \text{Solve for } M_i \text{ and } M_{i+1}. \quad i=1,2,3\ldots \tag{A18}$$

$$M_{avg_i} = \frac{M_i + M_{i+1}}{2} \qquad i=1,2,3\ldots \tag{A19}$$

$$P_{avg_i} = \frac{P_{0_{NE}}}{\left(1+\frac{\gamma-1}{2}M_{avg_i}{}^2\right)^{\frac{\gamma}{\gamma-1}}} \qquad i=1,2,3\ldots \tag{A20}$$

$$\alpha_i = \alpha_1 - \sin^{-1}\left(\sqrt{\frac{\frac{P_{DI}}{P_{avg}} - 1}{\gamma M_{avg}^2}}\right) \qquad i=1,2,3\ldots \tag{A21}$$

$$x_i = x_{i-1} + \cot(\alpha_{i-1})\,dr \qquad i=2,3,4\ldots \tag{A22}$$

5. DI to OS1: Calculate the conditions behind the impingement-induced oblique shock and its angle (β) using the diffuser inlet conditions and the angle of the plume boundary as it reaches the diffuser wall.

$$\theta_{IMP} = \alpha\,|_{r_{DI}} \tag{A23}$$

$$\tan(\theta_{IMP}) = 2\cot(\beta_{OS1})\left[\frac{M_{DI}^2\sin^2(\beta_{OS1})-1}{M_{DI}^2(\gamma+\cos(2\beta_{OS1}))+2}\right] \quad \text{Solve for } \beta_{OS1}. \quad \text{(A24)}$$

$$M_{n_1} = M_{DI}\sin(\beta_{OS1}) \quad \text{(A25)}$$

$$M_{n_2} = \sqrt{\frac{1+\frac{\gamma-1}{2}M_{n_1}^2}{\gamma M_{n_1}^2 - \frac{\gamma-1}{2}}} \quad \text{(A26)}$$

$$P_{OS1} = P_{DI}\left(1+\frac{2\gamma}{\gamma+1}(M_{n_1}^2-1)\right) \quad \text{(A27)}$$

$$M_{OS1} = \frac{M_{n_2}}{\sin(\beta_{OS1}-\theta_{IMP})} \quad \text{(A28)}$$

$$P_{0_{OS1}} = P_{OS1}\left(1+\frac{\gamma-1}{2}M_{OS1}^2\right)^{\frac{\gamma}{\gamma-1}} \quad \text{(A29)}$$

6. OS1 to OS2: Use the flow conditions found in the previous step to calculate the β of the contraction-induced oblique shock.

$$\tan(\theta_{DC}) = 2\cot(\beta_{OS2})\left[\frac{M_{OS1}^2\sin^2(\beta_{OS2})-1}{M_{OS1}^2(\gamma+\cos(2\beta_{OS2}))+2}\right] \quad \text{Solve for } \beta_{OS2}. \quad \text{(A30)}$$

$$M_{n_1} = M_{OS1}\sin(\beta_{OS2}) \quad \text{(A31)}$$

$$M_{n_2} = \sqrt{\frac{1+\frac{\gamma-1}{2}M_{n_1}^2}{\gamma M_{n_1}^2 - \frac{\gamma-1}{2}}} \quad \text{(A32)}$$

$$P_{OS2} = P_{OS1}\left(1+\frac{2\gamma}{\gamma+1}(M_{n_1}^2-1)\right) \quad \text{(A33)}$$

$$M_{OS2} = \frac{M_{n_2}}{\sin(\beta_{OS2}-\theta_{DC})} \quad \text{(A34)}$$

$$P_{0_{OS2}} = P_{OS2}\left(1+\frac{\gamma-1}{2}M_{OS2}^2\right)^{\frac{\gamma}{\gamma-1}} \tag{A35}$$

7. INT: Find the geometric point of intersection of the impingement and contraction oblique shocks.

$$x_{DC} = x_{NE}+2\left(\frac{L}{D}\right)_{DI} r_{DI} \tag{A36}$$

$$x_{INT} = \frac{x_{IMP}-x_{DC}\tan(\beta_{OS2})\cot(\beta_{OS1})}{1-\tan(\beta_{OS2})\cot(\beta_{OS1})} \tag{A37}$$

$$r_{INT} = r_{DI}-(x_{IMP}-x_{INT})\tan(\beta_{OS1}) \tag{A38}$$

$$r_{DC}|_{x_{INT}} = r_{DI}-\tan(\theta_{DC})(x_{INT}-x_{DC}) \tag{A39}$$

8. DI to NS: Assume a normal shock occupies the area between the two intersection points. Calculate mass flow rate through and P_0 behind the shock using diffuser inlet conditions.

$$\dot{m}_{NS} = P_{0_{DI}}(\pi r_{INT}^2)\sqrt{\frac{\gamma}{RT_0}}\left(1+\frac{\gamma-1}{2}\right)^{\frac{\gamma+1}{2(1-\gamma)}} \tag{A40}$$

$$P_{0_{NS}} = P_{0_{DI}}\left(1+\frac{\gamma-1}{2}M_{DI}^2\right)^{\frac{\gamma}{\gamma-1}} \tag{A41}$$

9. Subtract the mass flow through the normal shock from the system mass flow rate. Scale the P_0 of OS2 to give the resultant mass flow through the area between the shock intersection point and the diffuser wall. This forces conservation of mass. Make sure to correct the mass flow for the difference in the area normal and flow path along the wall.

$$\dot{m}_{OS2_{calculated}} = P_{0_{OS2}}\pi(r_{DI}-r_{INT})^2\cos^2(\theta_{DC})\sqrt{\frac{\gamma}{RT_0}}\left(1+\frac{\gamma-1}{2}\right)^{\frac{\gamma+1}{2(1-\gamma)}} \tag{A42}$$

$$P_{0_{OS2_{Forced}}} = P_{0_{OS2}} \frac{\left(\dot{m}_{system} - \dot{m}_{NS}\right)}{\dot{m}_{OS2_{calculated}}} \tag{A43}$$

10. OS2 & NS to ST: Apply an area-based weighted average of the two P_0 values to produce an estimate of the P_0 experienced at the inlet of the second throat.

$$P_{0_{weighted}} = \frac{P_{0_{NS}} r_{INT}^2 + P_{0_{OS2_{Forced}}} \left(r_{DC}|_{x_{INT}} - r_{INT}\right)^2}{\left(r_{DC}|_{x_{INT}}\right)^2} \tag{A44}$$

11. Determine the minimum second throat size based on the weighted P_0 using the isentropic mass flux equation.

$$A_{ST_{min}} = \frac{\dot{m}_{system}}{P_{0_{weighted}} \sqrt{\frac{\gamma}{RT_0}} \left(1 + \frac{\gamma - 1}{2}\right)^{\frac{\gamma+1}{2(1-\gamma)}}} \tag{A45}$$

The Isentropic Compression Model

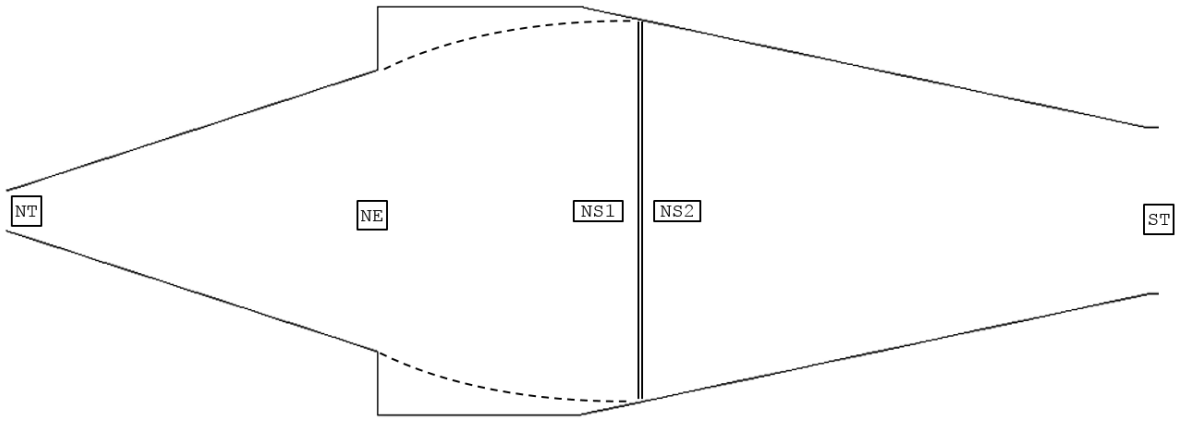

Fig. A2 – Calculation Locations for the Isentropic Compression Model

1. NT: Calculate the mass flow rate of the system with the isentropic mass flux equation applied at the nozzle throat.

$$\dot{m}_{system} = (P_0 A)_{NT} \sqrt{\frac{\gamma}{RT_0}} \left(1+\frac{\gamma-1}{2}\right)^{\frac{\gamma+1}{2(1-\gamma)}} \tag{A46}$$

2. NT to NE: Assume isentropic expansion through the nozzle to find the flow conditions at the nozzle exit.

$$P_{0_{NE}} = P_{0_{NT}} \tag{A47}$$

$$\frac{A_{NE}}{A_{NT}} = \left(\frac{1}{M_{NE}}\right)\left(\frac{1+\frac{\gamma-1}{2}M_{NE}^2}{\frac{\gamma+1}{2}}\right)^{\frac{\gamma+1}{2(\gamma-1)}} \qquad \text{Solve for } M_{NE}. \tag{A48}$$

$$P_{NE} = \frac{P_{0_{NE}}}{\left(1+\frac{\gamma-1}{2}M_{NE}^2\right)^{\frac{\gamma}{\gamma-1}}} \tag{A49}$$

3. NE to NS1: Conical nozzle thrust efficiency is essentially the percentage of the total flow momentum being ejected in the axial direction. As such, it can be used to find the average flow half-angle at nozzle exit. Assume isentropic compression from the average flow half-angle to axial flow right before the normal shock. Use an inverse Prandtl-Meyer expansion to find the Mach number after the turn and the isentropic relations to define the resultant flow conditions.

$$\eta = \frac{1}{2}\left(1+\cos(\theta_{NE})\right) \tag{A50}$$

$$\theta_{avg} = \tan^{-1}\left(\frac{1-\eta}{\eta}\right) \tag{A51}$$

$$\nu_{NE} = \sqrt{\frac{\gamma+1}{\gamma-1}}\tan^{-1}\sqrt{\frac{\gamma-1}{\gamma+1}(M_{NE}^2-1)} - \tan^{-1}\sqrt{M_{NE}^2-1} \tag{A52}$$

$$\nu_{NS1} = \nu_{NE} - \theta_{avg} \tag{A53}$$

$$\nu_{NS1} = \sqrt{\frac{\gamma+1}{\gamma-1}}\tan^{-1}\sqrt{\frac{\gamma-1}{\gamma+1}(M_{NS1}^2-1)} - \tan^{-1}\sqrt{M_{NS1}^2-1} \qquad \text{Solve for } M_{NS1}. \quad \text{(A54)}$$

4. NS1 to NS2: Pass the isentropically-compressed flow through a normal shock and find the post-shock P_0.

$$P_{0_{NS2}} = P_{0_{NE}}\left[\frac{\frac{\gamma+1}{2}M_{NS1}^2}{1+\frac{\gamma-1}{2}M_{NS1}^2}\right]^{\frac{\gamma}{\gamma-1}}\left[\frac{1}{\frac{2\gamma}{\gamma+1}M_{NS1}^2 - \frac{\gamma-1}{\gamma+1}}\right]^{\frac{1}{\gamma-1}} \qquad \text{(A55)}$$

5. NS2 to ST: Determine the second throat size based on the post-shock P_0 and system mass flow rate.

$$A_{ST_{min}} = \dot{m}\left[P_{0_{NS2}}\sqrt{\frac{\gamma}{RT_0}}\left(1+\frac{\gamma-1}{2}\right)^{\frac{\gamma+1}{2(1-\gamma)}}\right]^{-1} \qquad \text{(A56)}$$